High-Throughput Bioprinting of Spheroids for Scalable Tissue Fabrication

Myoung Hwan Kim[1,2], Yogendra Pratap Singh[2,3], Nazmiye Celik[2,3], Miji Yeo[2,3], Elias Rizk[4], Daniel J. Hayes[1,2,5], and Ibrahim T. Ozbolat[1,2,3,4,5,6*]

[1] Department of Biomedical Engineering, Penn State University, University Park, PA, USA

[2] The Huck Institutes of the Life Sciences, Penn State University, University Park, PA, USA

[3] Engineering Science and Mechanics Department, Penn State University, University Park, PA, USA

[4] Department of Neurosurgery, Penn State Milton S. Hershey Medical Center, Hershey, PA, USA

[5] Materials Research Institute, Penn State University, University Park, PA, USA

[6] Department of Medical Oncology, Cukurova University, Adana, Turkey

[*] Author to whom any correspondence should be addressed. Email: ito1@psu.edu

This PDF includes:

Supplementary Figs. 1-19

Supplementary Tables 1-2

Supplementary Notes 1-2

Supplementary Figures

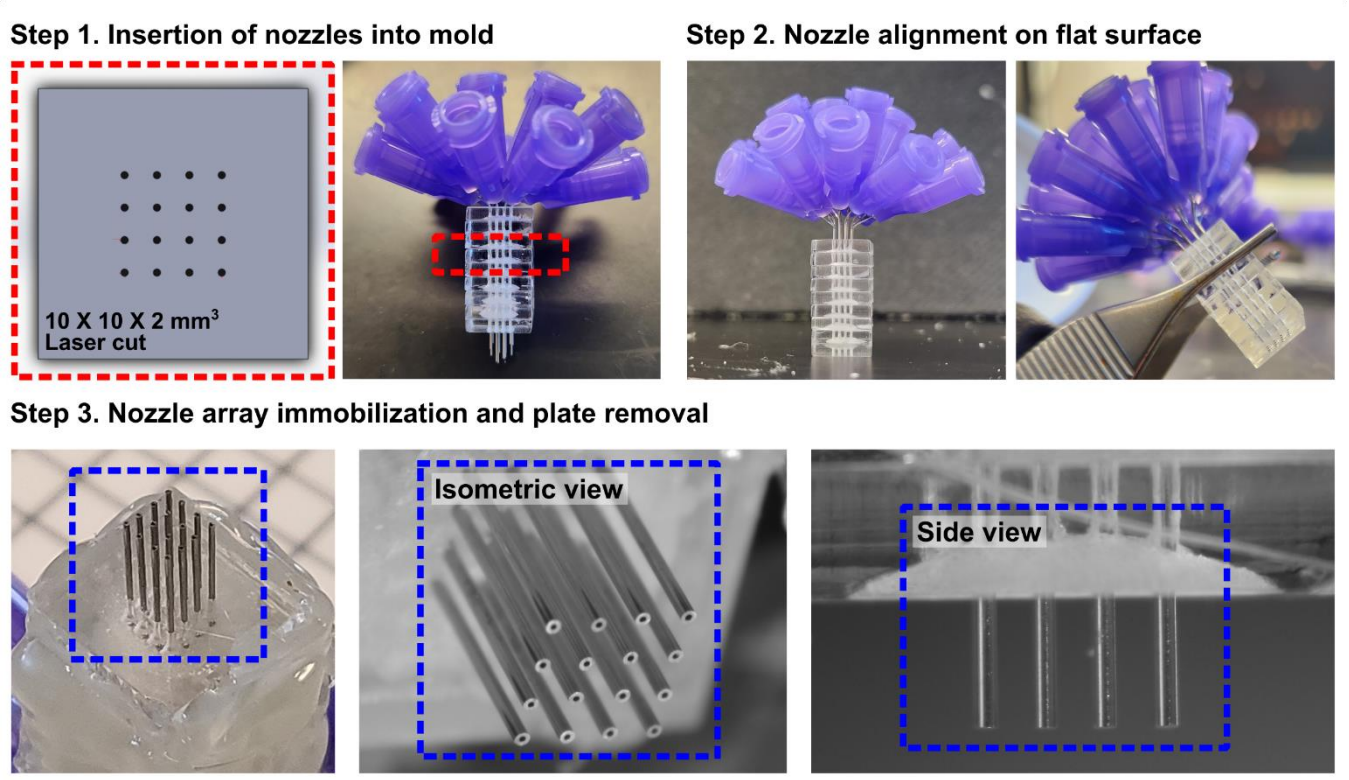

Supplementary Fig. 1. Schematics illustrating the preparation of the DCNA nozzle. First, nozzles were inserted into precisely stacked acrylic plates, micro-manufactured via laser cutting. Next, the nozzles were levelled and aligned by pressing them against a flat surface. An adhesive was then applied to immobilize the assembled nozzles. Finally, the two bottom acrylic plates were removed to obtain DCNA.

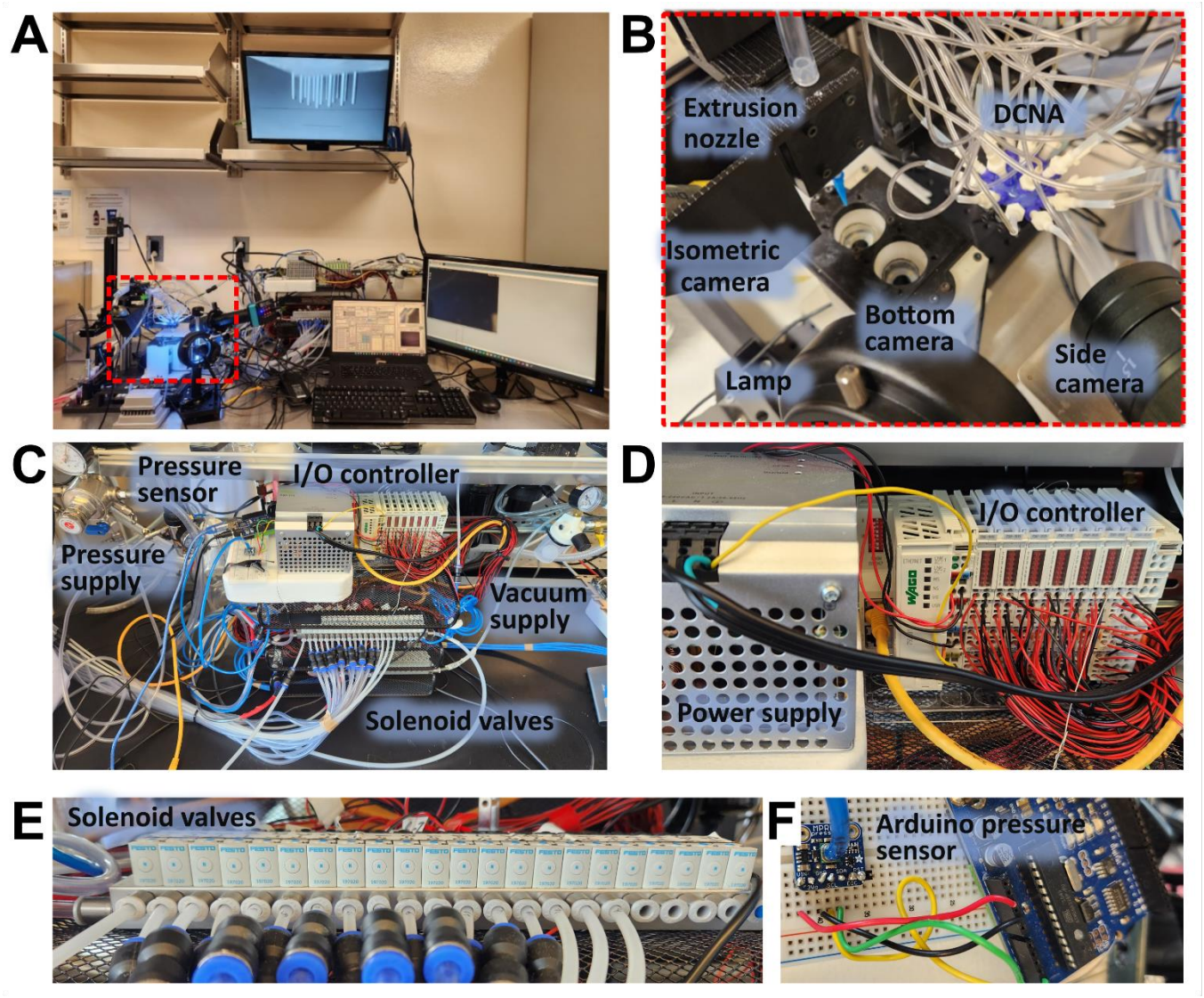

Supplementary Fig. 2. HITS-Bio hardware setup for (A) intraoperative bioprinting in a surgical setting. (B) HITS-Bio was composed of DCNA associated with an extrusion nozzle, cameras for isometric, side, and bottom views. (C) The components involved in pressure control, including the pressure sensor, pressure supply, vacuum supply, and solenoid valves were used for regulation of pressure/vacuum. (D) Input/output (I/O) controller and power supply, which manage the electronic control aspects of the system. (E) Solenoid valves, essential for regulating the pressure and vacuum in DCNA. (F) Arduino pressure sensor setup was utilized for real-time monitoring of pressure within the system.

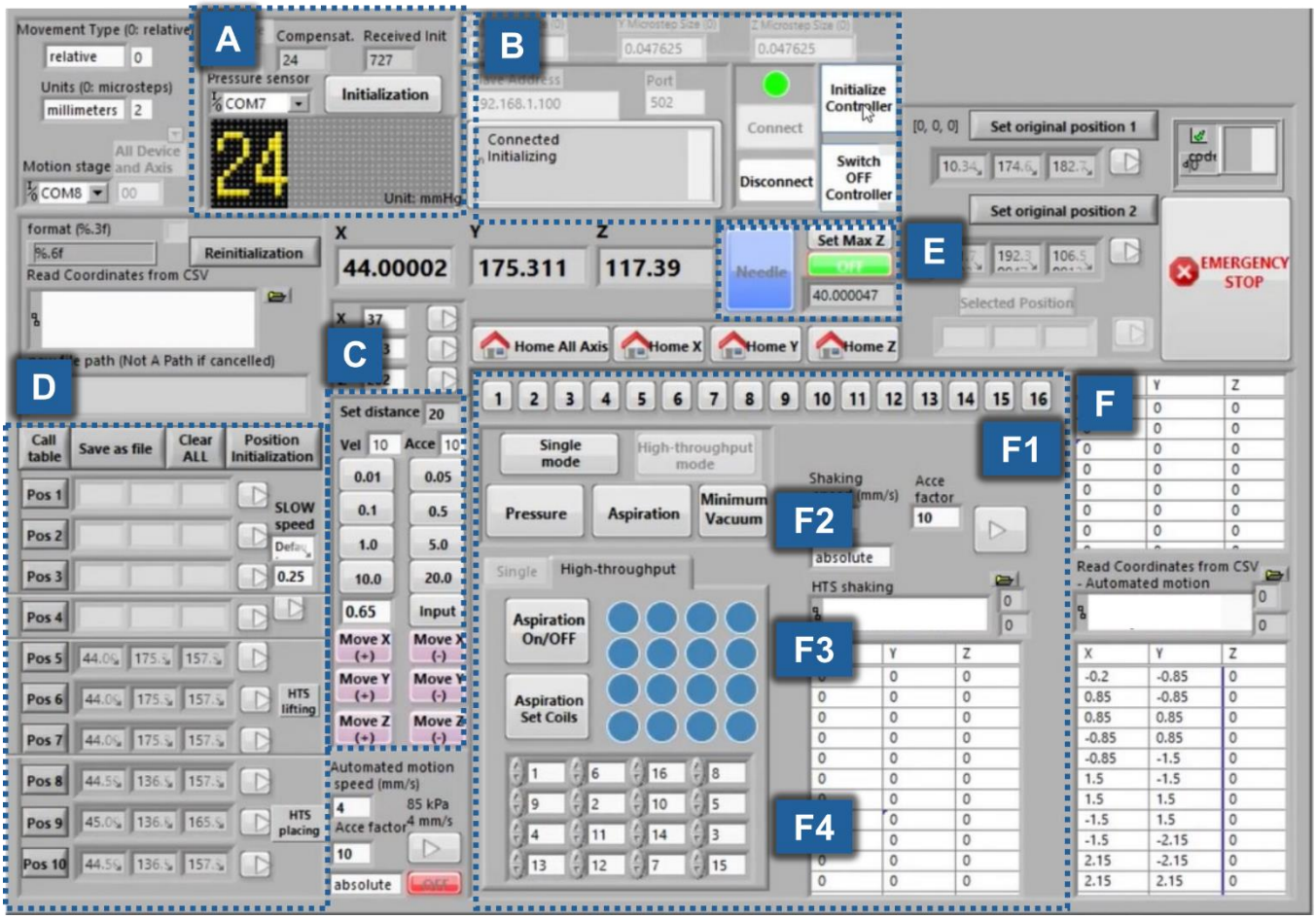

Supplementary Fig. 3. Software interface setup marked into Panels A-F. Descriptions for each Panel on the interface were provided in **Supplementary Note 2**.

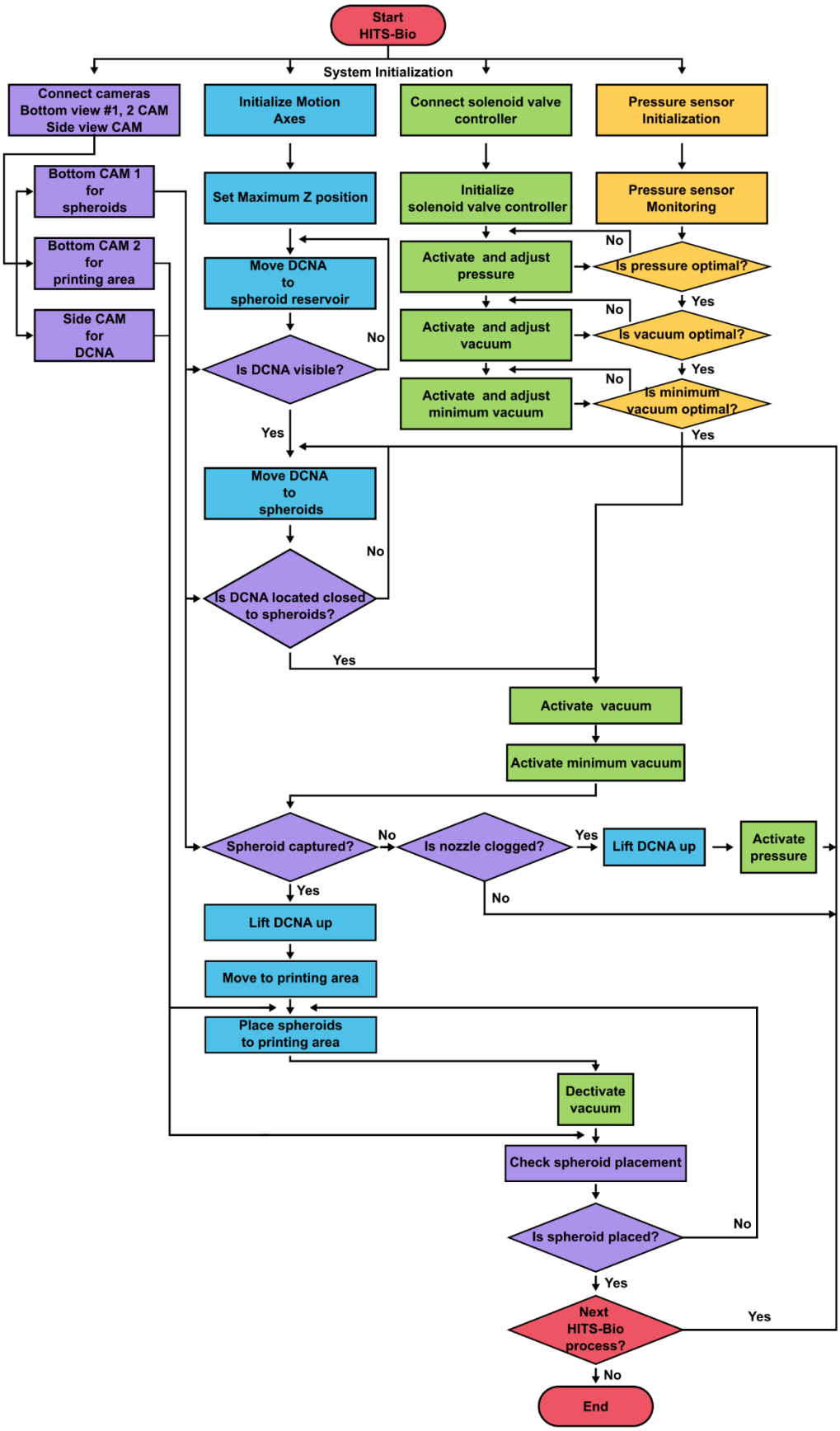

Supplementary Fig. 4. A detailed control algorithm for the HITS-Bio operation.

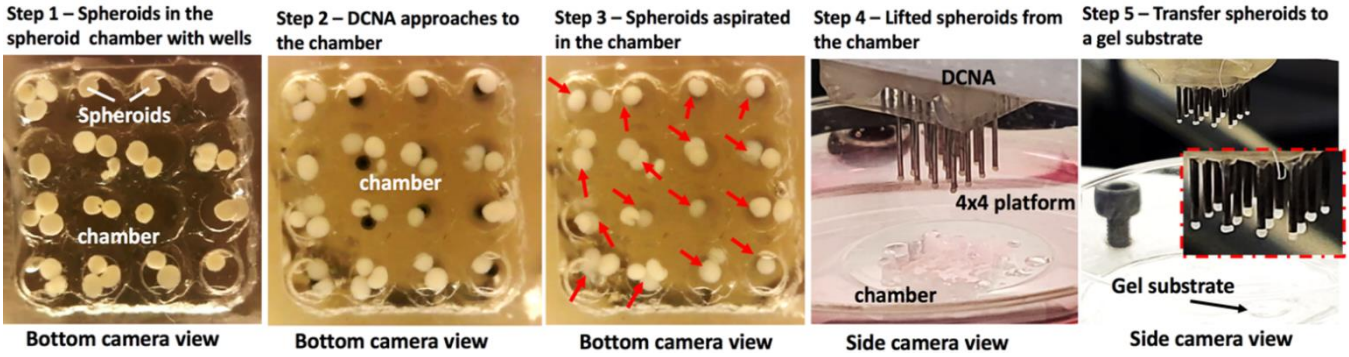

Supplementary Fig. 5. The HITS-Bio process. Steps involved in loading spheroids. Spheroids were picked up from a spheroid chamber filled with a cell culture medium via selectively aspirating them and then transferred to a location for bioprinting onto a gel substrate. Red arrows demonstrate loaded spheroids.

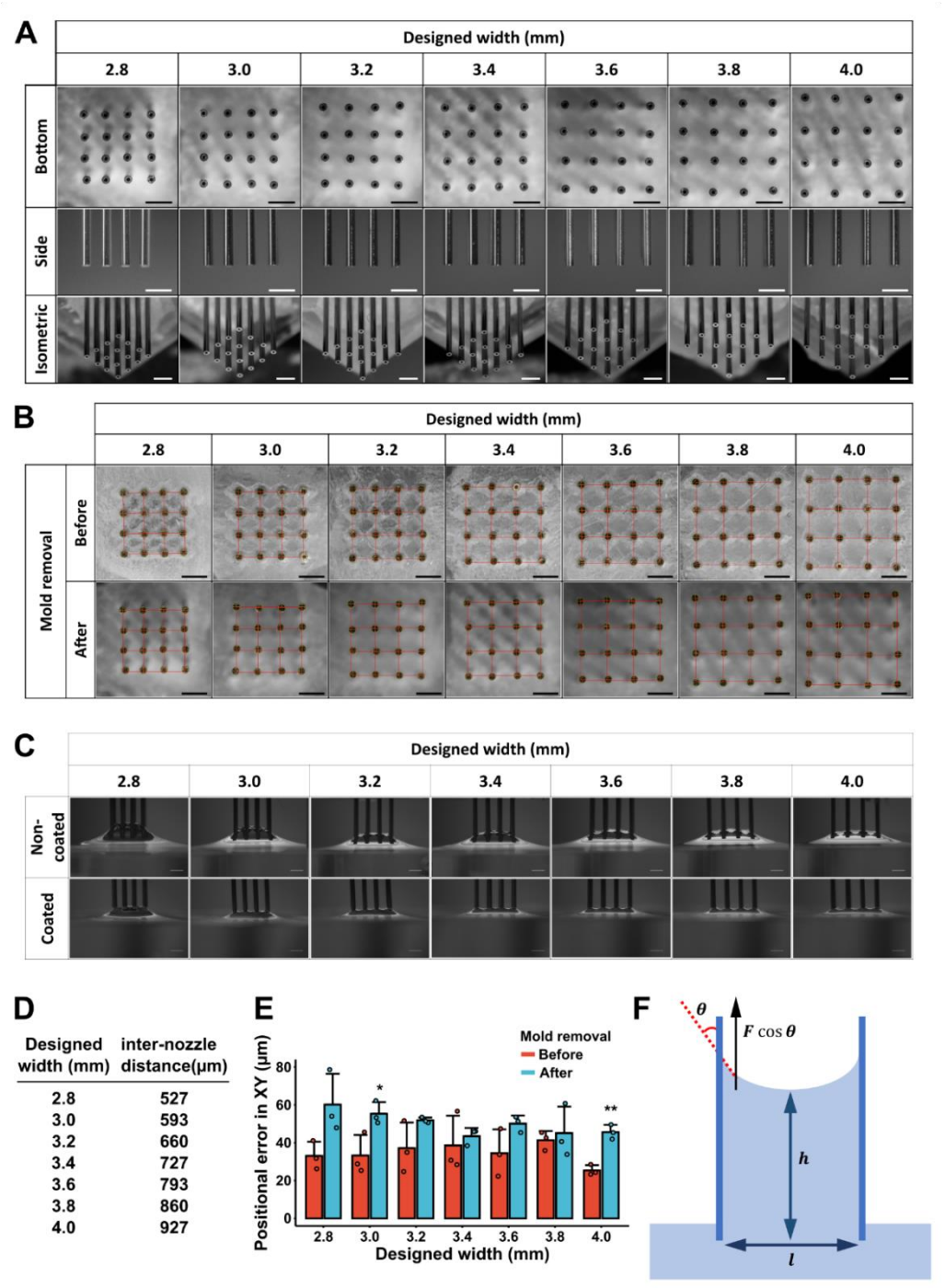

Supplementary Fig. 6. (A) Bottom, side, and isometric views of DCNA with varying designed widths. Scale bar: 1 mm. (B) Pictorial representation of the positional error before and after the mold removal calculated by any deviation from the ideal grid (red) and the centre of the nozzle (scale bar: 1 mm). (C) Side view of liquid elevation in DCNA to evaluate the effect of silicon coating on DCNA. Scale bar: 1 mm. (D) Inter-nozzle distance of DCNA ranging from 2.8 to 4.0 mm in width. (E) Quantified positional error in XY of DCNA with different designed widths before and after mold removal (n = 3, each data point represents the average positional error in XY from three independent DCNA before and after mold removal, unpaired two-sided Student's t-test, p = 0.05846, 0.03725, 0.13499, 0.63407, 0.11140, 0.68016, 0.00176, from left to right). Source data are provided as a Source Data file. (F) A schematic demonstration to describe the liquid elevation in DCNA and related parameters. Data are presented as mean ± SD where *p < 0.05 and **p < 0.01.

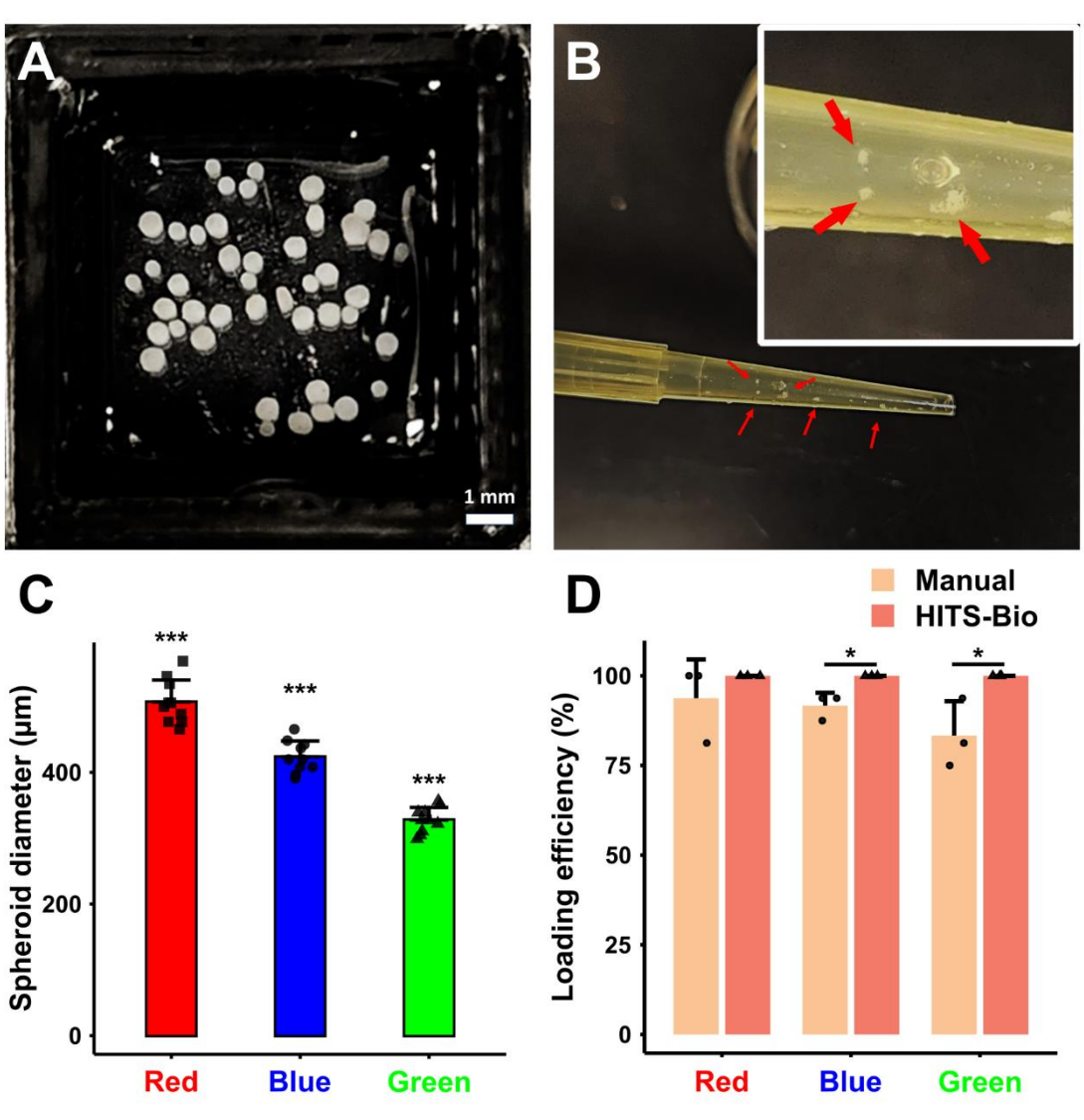

Supplementary Fig. 7. (A) Manually loaded different types (size and fluorescently labelled (color)) of spheroids loaded on 10% GM, followed by photo-crosslinking. (B) Red arrow indicates spheroids attached inside the pipette tip while mixing process without extrusion. (C) Diameter of spheroids stained with different colors (n = 10 biologically independent samples, one-way ANOVA, all shown comparisons $p < 0.0001$), (D) Comparison of loading efficiency (%) for manually loaded spheroids vs. HITS-Bio bioprinted spheroids for each color (n = 3 biologically independent samples, unpaired two-sided Student's t-test, p = 0.37390, 0.03902, 0.01613, from left to right). Data are presented as mean ± SD where *p < 0.05 and ***p < 0.001. Source data are provided as a Source Data file.

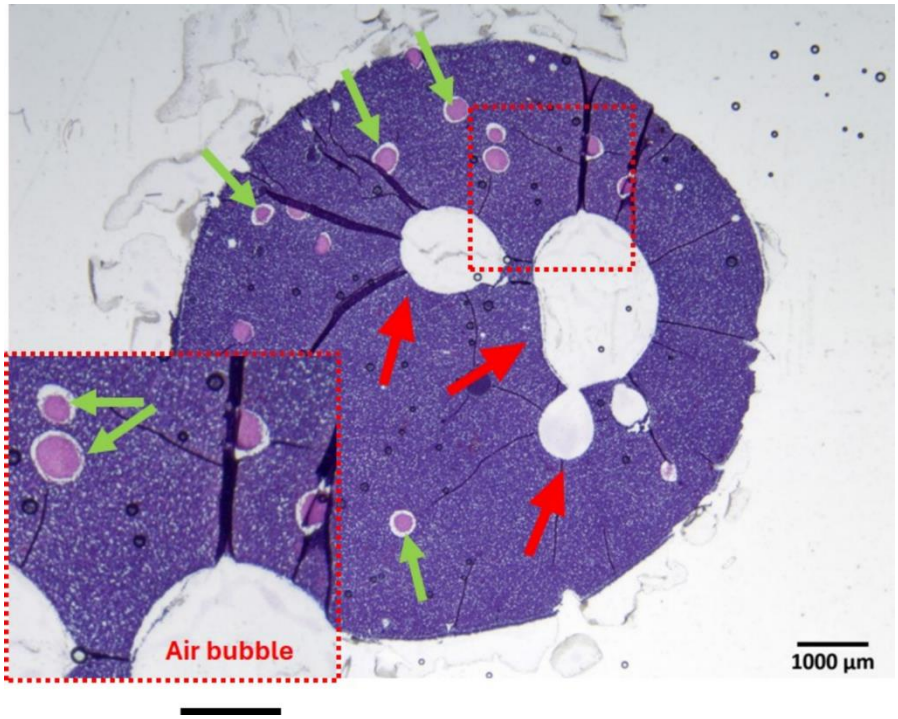

Supplementary Fig. 8. H&E-stained images of the manually fabricated group, where 64 spheroids were randomly mixed into the BONink and extruded into a well plate. Green arrows indicate spheroids while red arrows highlight the formation of air bubbles.

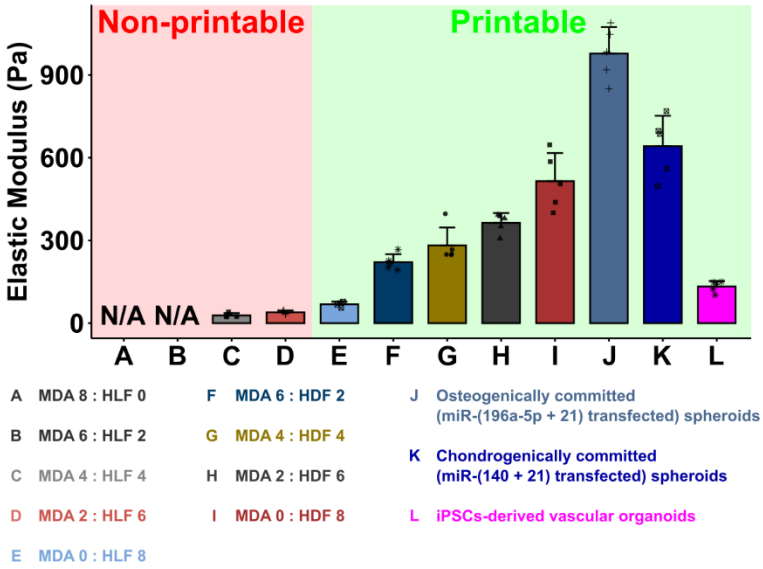

Supplementary Fig. 9. The range of elastic moduli of spheroids and organoids in which they were effectively bioprinted using HITS-Bio (n = 4, 4, 4, 4, 4, 5, 5, 5, 5, 5, 5, 5 biologically independent samples, from left to right). The x-axis represents various spheroid/organoid types, each prepared using a total of 8,000 cells. (A-I) The different ratios of MDA-MB-231 cells (MDA), human lung fibroblasts (HLF), and human dermal fibroblasts (HDF), (J) osteogenically-committed spheroids, (K) chondrogenically-committed spheroids and (L) iPSC-derived vascular organoids. Data are presented as mean ± SD. Source data are provided as a Source Data file.

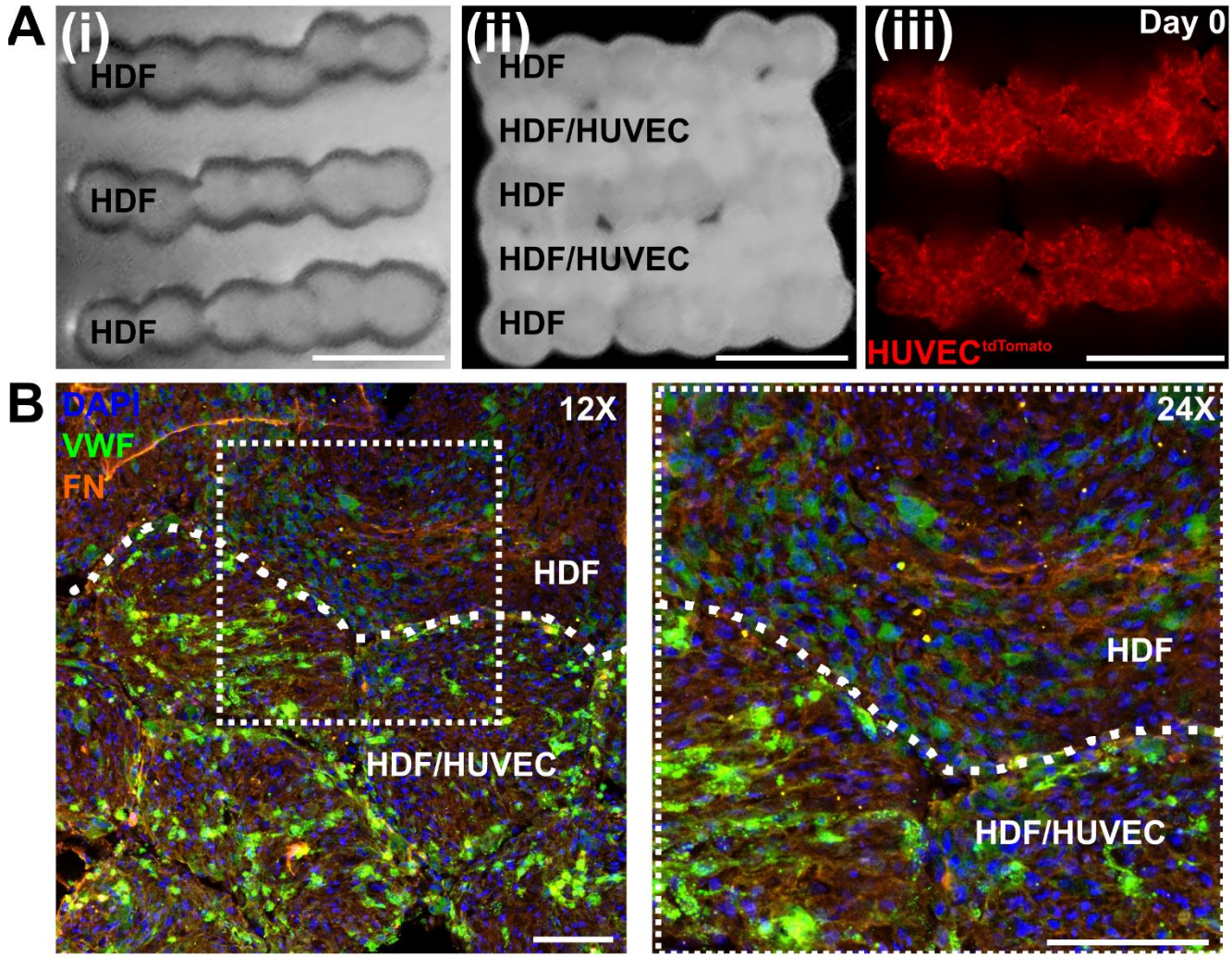

Supplementary Fig. 10. Demonstration of fully cellular, tightly packed constructs. (A) Phase-contrast images showing (i) HDF spheroids deposited in rows, (ii) HDF/HUVEC spheroids deposited between the rows to achieve complete packing, and (iii) fluorescence images of a construct showing distribution of tdTomato$^+$ HUVECs (scale bar: 1 mm). (B) Sections stained with VWF (green), FN (orange), and DAPI (blue), highlighting the interface of fusion (indicated by the white dashed line) after 3 days of culture (scale bar: 100 µm).

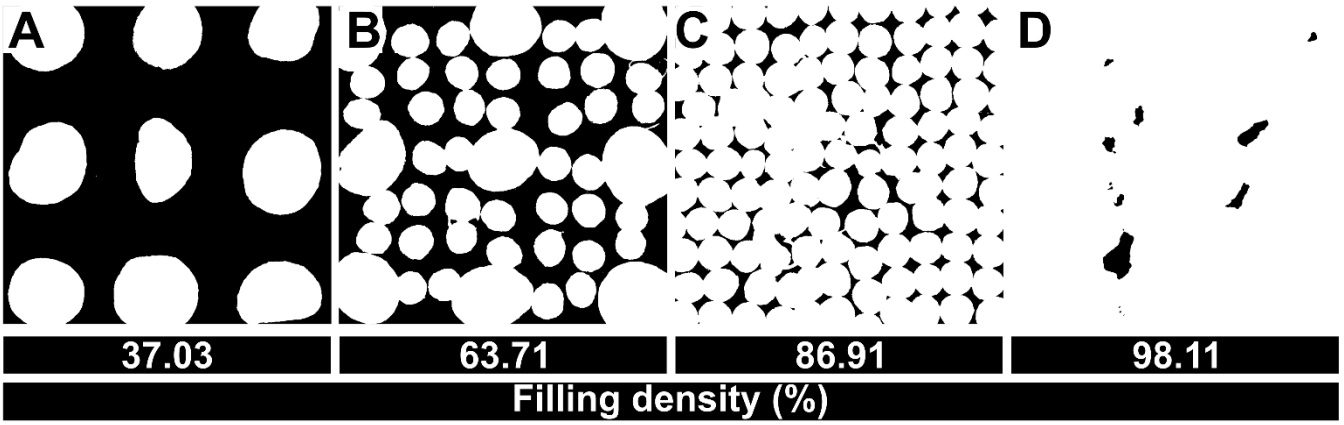

Supplementary Fig. 11. Optimization of area filling in tissue constructs using HITS-Bio. Area filling using (A) large (~735 µm) spheroids, (B) a mixture of large (~735 µm) and small (~300 µm) spheroids, (C) small (~300 µm) spheroids alone, and (D) by combining two different spheroid sizes (~530 and ~300 µm).

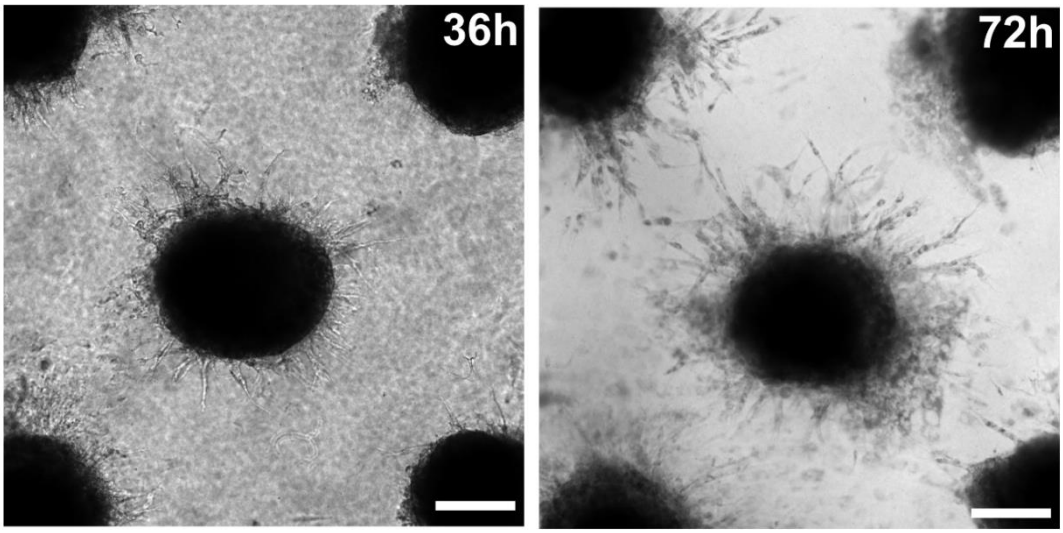

Supplementary Fig. 12. Optical microscopic images of bioprinted iPSC-derived vascular organoids after 36 and 72 h (scale bar: 200 µm). The center organoid (~400 µm in diameter) was placed at a center-to-center distance of ~800 µm from the organoids at the corners.

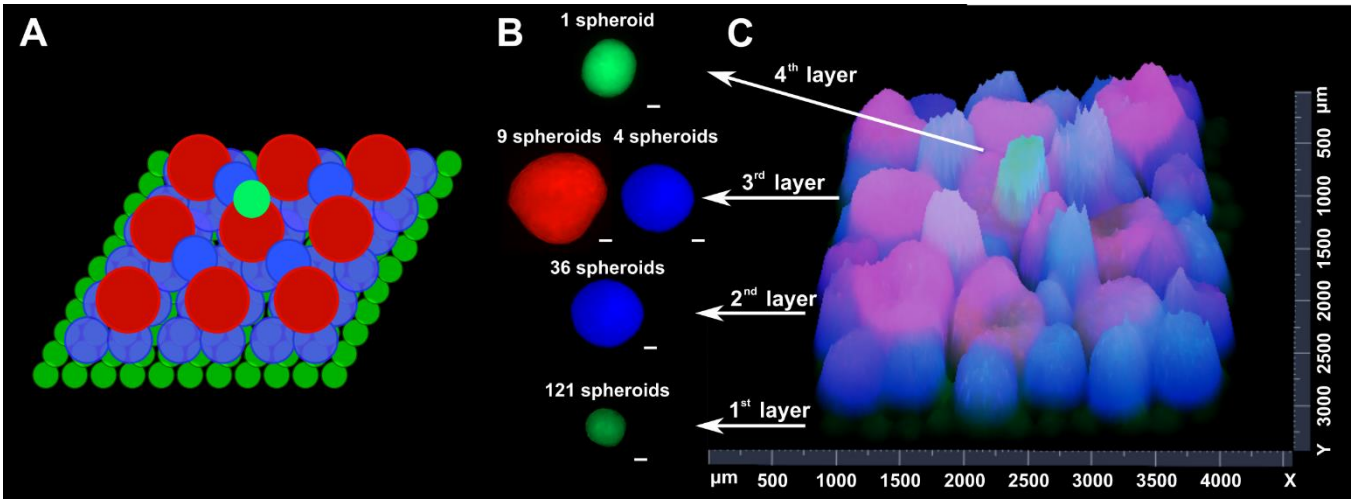

Supplementary Fig. 13. A multi-layered pyramid-like construct. (A) Schematic representation of the construct (B) with different spheroid sizes and their color-coded tags (scale bar: 100 µm), and (C) 2.5D rendered image of the assembled construct.

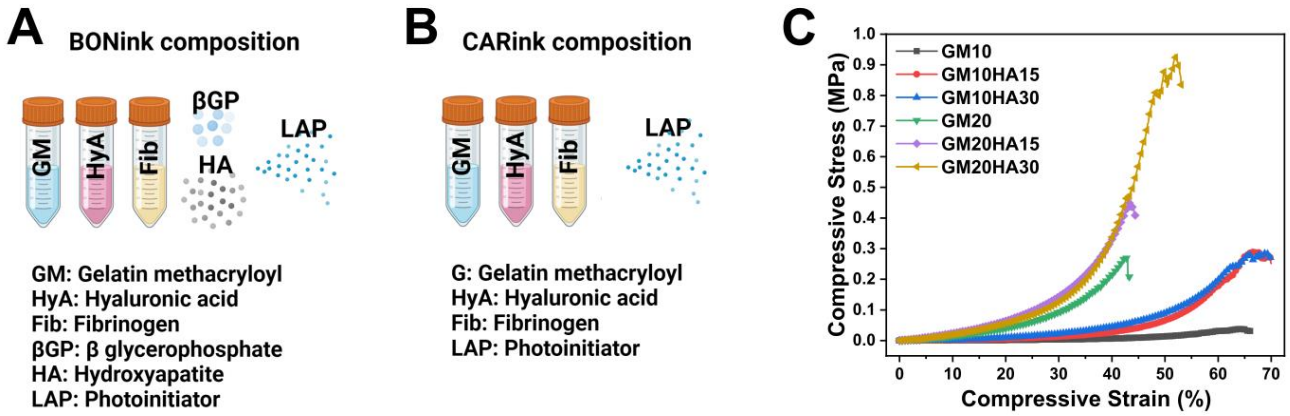

Supplementary Fig. 14. (A) BONink components, (B) CARink components, and (C) compressive stress of BONink and CARink with different concentrations of GM and HA. Source data are provided as a Source Data file. (A) and (B) were created in BioRender. Ozbolat, I. (2023) BioRender.com/u48v904.

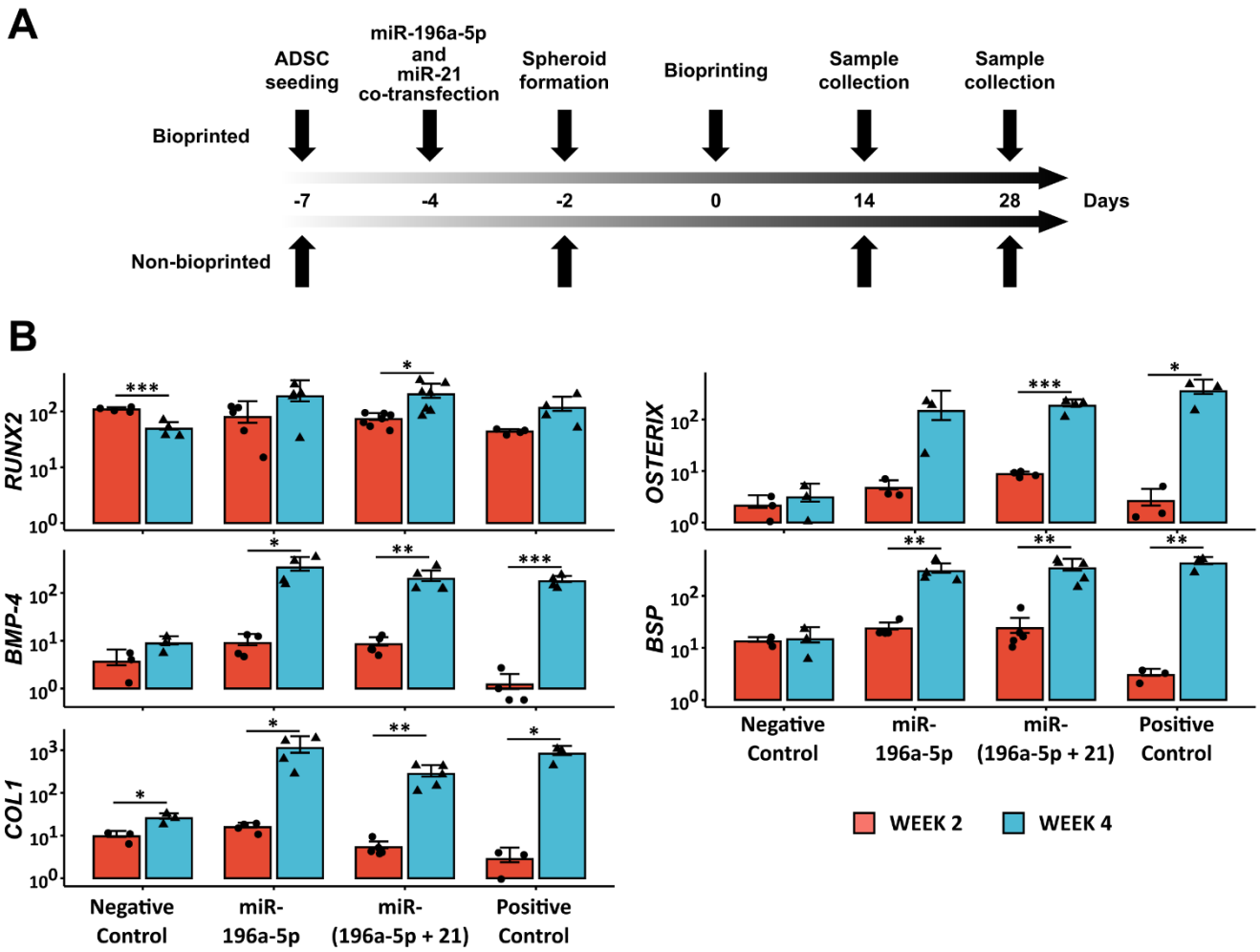

Supplementary Fig. 15. (A) A schematic describing the timeline and preparation of miRNA transfection and sample collection. (B) Quantitative gene expression of non-transfected ADSCs spheroids (negative control), miR-transfected spheroids and spheroids of ADSCs cultured with the osteogenic differentiation medium (positive control) at Weeks 2 and 4, normalized with respect to non-transfected ADSCs at Day 1 (*RUNX2*: $n = 4, 5, 7, 4$ biologically independent samples (from left to right), unpaired two-sided Student's t-test, $p = 0.00067, 0.05789, 0.01004, 0.06940$ (from left to right); *BMP-4*: $n = 3, 4, 5, 4$ biologically independent samples (from left to right), unpaired two-sided Student's t-test, $p = 0.08304, 0.01796, 0.00505, 0.00044$ (from left to right); *COL1*: $n = 3, 4, 5, 3$ biologically independent samples (from left to right), unpaired two-sided Student's t-test, $p = 0.02349, 0.03119, 0.00395, 0.01381$ (from left to right); *OSTERIX*: $n = 3, 3, 4, 3$ biologically independent samples (from left to right), unpaired two-sided Student's t-test, $p = 0.51080, 0.08831, 0.00041, 0.02696$ (from left to right); *BSP*: $n = 3, 4, 5, 3$ biologically independent samples (from left to right), unpaired two-sided Student's t-test, $p = 0.81494, 0.00725, 0.00147, 0.00389$ (from left to right)). Data are presented as mean ± SD where $*p < 0.05$, $**p < 0.01$, and $***p < 0.001$. Source data are provided as a Source Data file.

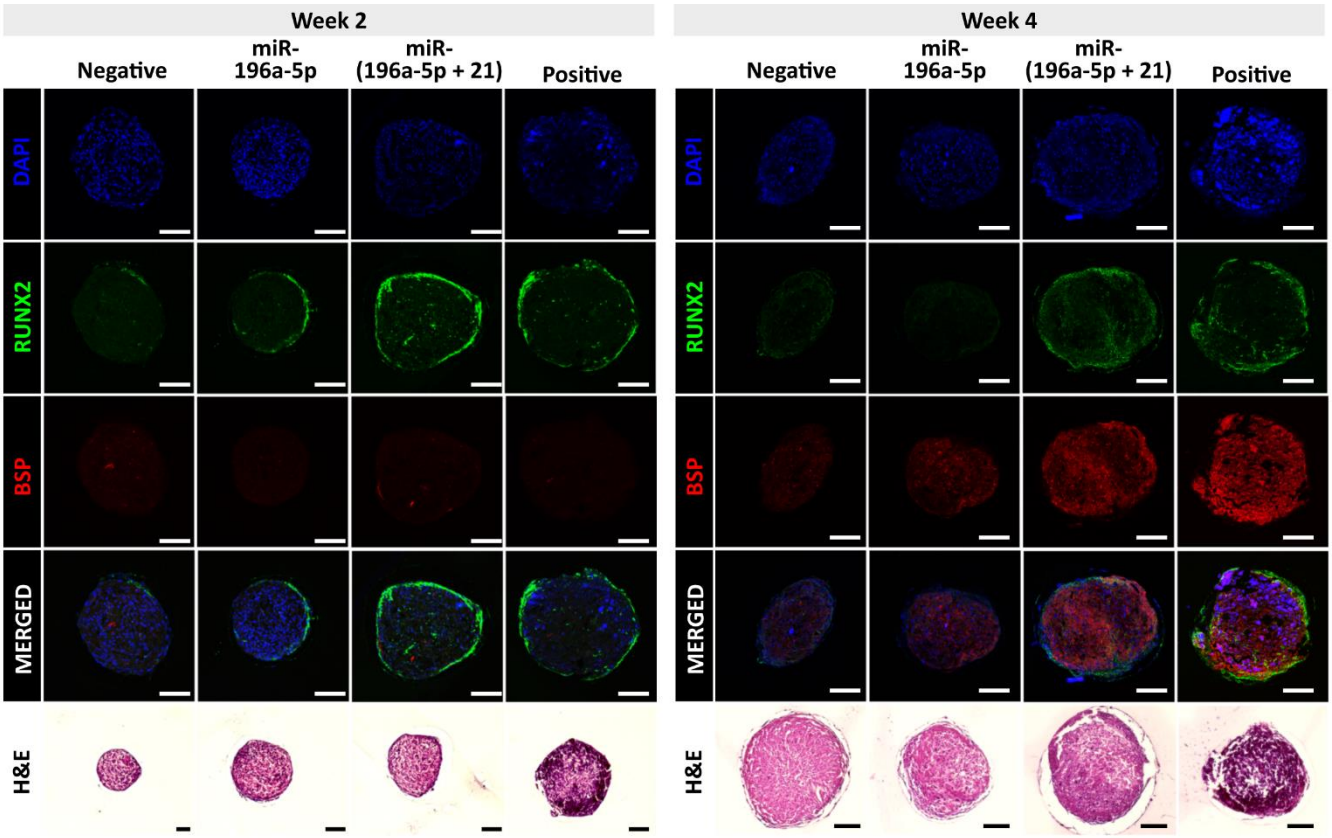

Supplementary Fig. 16. IHC images of non-transfected and transfected hADSC spheroids stained with RUNX2, BSP, and H&E at Weeks 2 and 4 (scale bars, 100 µm).

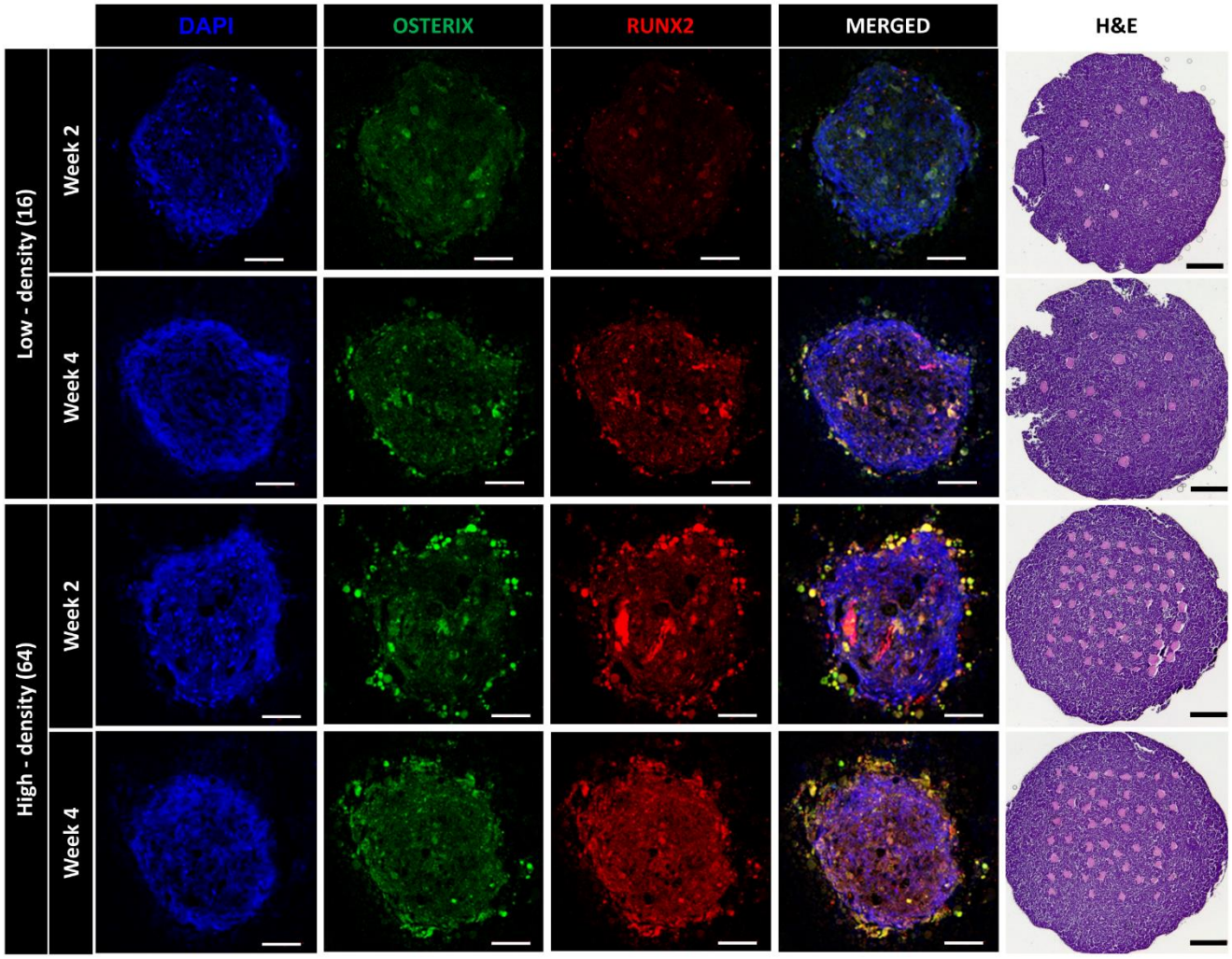

Supplementary Fig. 17. IHC (scale bar: 100 µm) and H&E (scale bar: 1 mm) images of bioprinted bone tissue with two different densities (low and high) at Weeks 2 and 4.

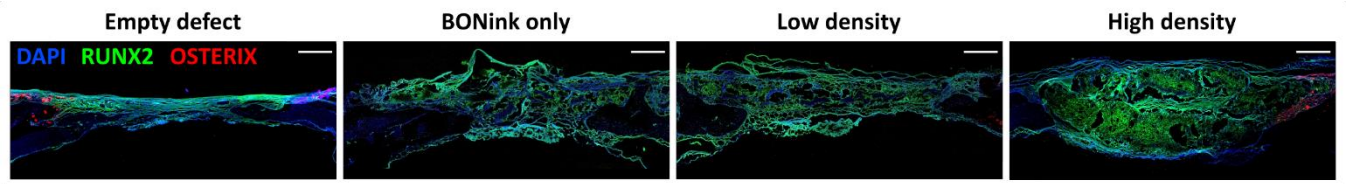

Supplementary Fig. 18. IHC images of retrieved explants (after 6 weeks) stained for RUNX2 (green), OSTERIX (red) and DAPI (blue) (scale bar: 500 µm).

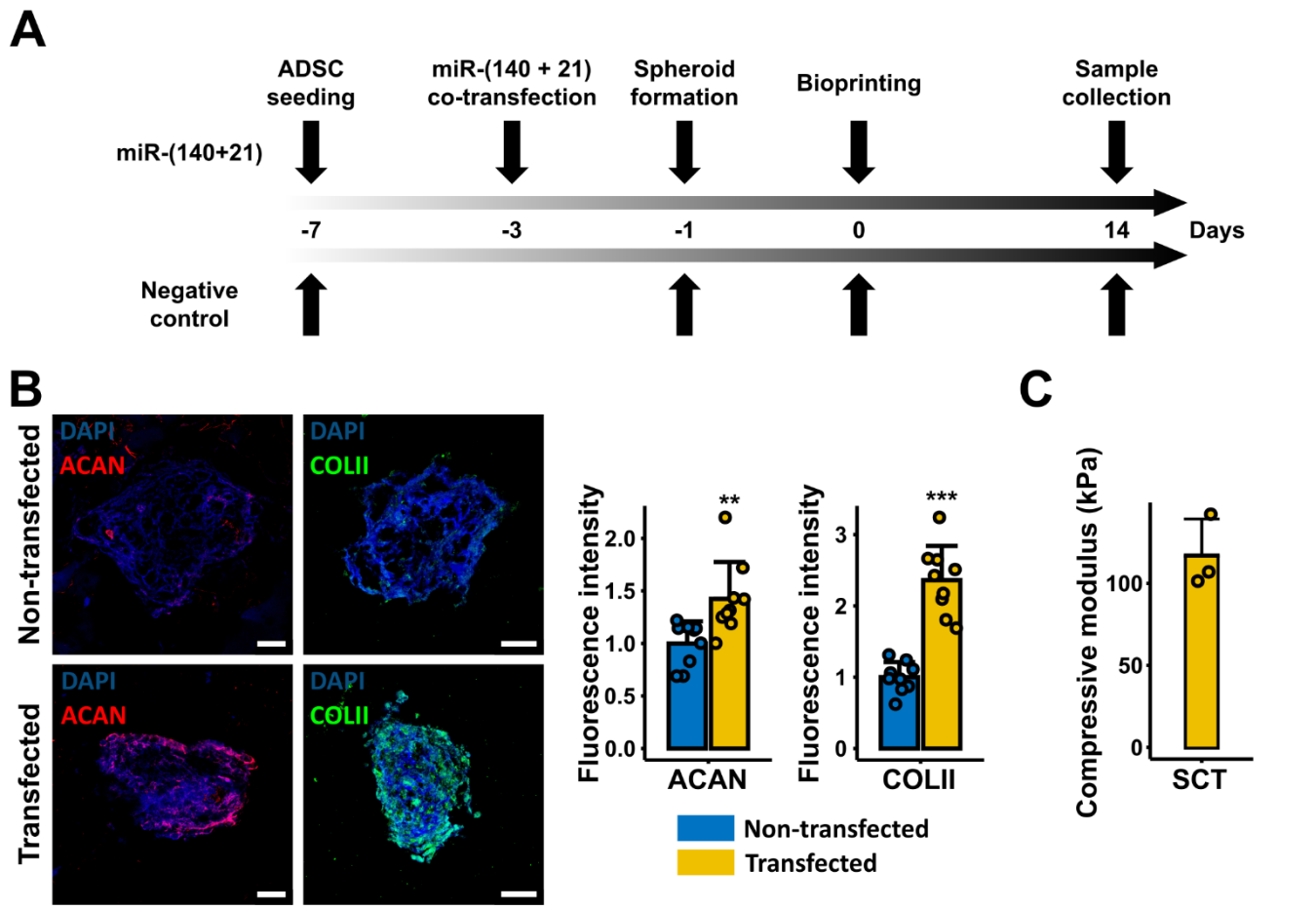

Supplementary Fig. 19. (A) A schematic describing the timeline and preparation of miRNA transfection and sample collection for SCT fabrication. (B) IHC with ACAN and COLII for non-transfected and transfected spheroids in cm^3 cartilage tissues at Week 2 and their fluorescence intensity ($n = 9$ biologically independent samples, unpaired two-sided Student's t-test, ACAN $p = 0.00665$, COLII $p = 7.9 \times 10^{-7}$). Scale bar: 50 µm. (C) Compressive modulus of the bioprinted SCTs ($n = 3$ biologically independent samples). Data are presented as mean ± SD where $^{**}p < 0.01$ and $^{***}p < 0.001$. Source data are provided as a Source Data file.

Supplementary Tables

Supplementary Table 1. Fold change in gene expression for osteogenic marker on Week 4 as compared to Week 2, normalized to negative control (non-transfected hADSCs on Day 1).

Markers	2D Transfection	Transfected Spheroids	HITS-Bio Low Density	HITS-Bio High Density
RUNX2	2.3	2.7	4.8	1.1
BMP-4	7.4	23.3	1.8	2.4
COL1	2.3	52.1	5.1	2.5
OSTERIX	26.5	21.3	6.1	15.4
BSP	1.3	14.1	8.6	9.6

Supplementary Table 2. Primers of the genes used in the qRT-PCR study.

Gene	Forward primer	Reverse primer
COL1	ATG ACT ATG AGT ATG GGG AAG CA	TGG GTC CCT CTG TTA CAC TTT
RUNX2	GGT TAA TCT CCG CAG GTC ACT	CAC TGT GCT GAA GAG GCT GTT
BSP	AAC GAA GAA AGC GAA GCA GAA	TCT GCC TCT GTG CTG TTG GT
BMP-4	TAG CAA GAG TGC CGT CAT TCC	GCG CTC AGG ATA CTC AAG ACC
OSTERIX	CCT CTG CGG GAC TCA ACA AC	AGC CCA TTA GTG CTT GTA AAG G
GAPDH	CAC ATG GCC TCC AAG GAG TA	GTA CAT GAC AAG GTG CGG CT

Supplementary Notes

Supplementary Note 1. Capillary reaction in DCNA

A capillary reaction was observed between nozzles (**Supplementary Fig. 6F**), where liquid rises in a narrow gap against gravity. The surface tension of the liquid was calculated based on the height of elevated liquid, gravity, density of the liquid, and the inter-nozzle distance of DCNA. At equilibrium, the upward force must balance the downward force. The upward force pulls a specific volume of liquid upward, equivalent to the weight of the lifted liquid:

$$F_{st}\cos\theta = \gamma_{st}L = F_{weight} \quad (1)$$

where, F_{weight} is force from the weight of the liquid pulled up, and γ_{st} is the coefficient of surface tension of liquid (water- 0.0727 N/m at 20 °C). L is the length of the boundary between the liquid and surface along with the surface tension acts (**Supplementary Fig. 6F**). This can be simplified as F_{weight} is equal to mg, where m is mass and g is gravitational force. The liquid continues to elevate until the force from the surface tension equals the weight of the liquid pulled up above the original liquid level:

$$\gamma_{st} \times 4l = mg \quad (2)$$

And since $m = \rho V$, where ρ is the density and V is the volume of the lifted liquid, equation (2) can be rewritten as:

$$\gamma_{st} \times 4l = \rho V g \quad (3)$$

Since V is the volume surrounded by nozzles in DCNA and is equal to l^2h, where l is inter-nozzle distance and h is the height of the elevated liquid:

$$\gamma_{st} \times 4l = \rho l^2 h g \quad (4)$$

Equation (4) can be rearranged to:

$$h = \frac{4\gamma_{st}}{\rho l g} \quad (5)$$

Here, equation (5) is the relationship between the surface tension, elevated liquid height, and inter-nozzle distance in DCNA. Here, two parameters can be altered to decrease *h*: either increasing l or decreasing γ_{st}.

Supplementary Note 2. Software Interface and Control Algorithm

The control algorithms for the DCNA involved several key functions to ensure precise operation and safe handling of spheroids. For better understanding, the software interface was marked into different Panels A-F (**Supplementary Fig. 3**).

Positioning: The DCNA was mounted on the Z-axis and moved using keyboard arrow keys. The arrow keys moved the X and Y axes, while the Page Up and Page Down keys move the Z-axis. Users can set the step size, ranging from 0.01 to 20 mm, via designated buttons in Panel C. For a customized step size, users can input values followed by pressing the 'Input' button. Additionally, velocity and acceleration parameters were entered in the 'Vel' and 'Acce' fields within the same Panel.

Saving and Retrieving Positions: Users can save up to ten positions during the operation by pressing the corresponding 'Pos #' button in Panel D after setting the DCNA's coordinates. These saved positions can be easily accessed and moved by clicking the play buttons next to each position button in Panel D.

Safety Controls: To ensure that spheroids were not damaged during handling, a maximum Z position was set by pressing the 'Set Max Z' button once the DCNA reached the required height. This position was entered and activated by toggling the activation switch in Panel E to prevent potential damage to spheroids and DCNA.

Pressure and Aspiration Controls: Pressure levels, aspiration, and minimum vacuum were controlled via buttons in Panel F2. The 'Minimum Vacuum' button was specifically designed to hold aspirated media and to prevent leakage when spheroids were placed. Real-time monitoring of these pressure values was available in Panel A., The 'Initialization' button in Panel A calibrates the pressure sensor to zero.

Solenoid Valve Connection: The interface included a direct connection to the solenoid valve controller, displayed in Panel B. Users can connect or disconnect the controller with 'Connect' and 'Disconnect' buttons, respectively. The 'Initialize Controller' button resets the controller and closes all valves, while the 'Switch OFF Controller' opens all of them to turn off the controller.

Nozzle Configuration and Operation: Individual nozzles on DCNA can be controlled via buttons labeled '1' to '16' in Panel F1. The arrangement of these nozzles into a desired array was set in Panel F4, and their positions were confirmed through a camera view matched to a 4 x 4 light-emitting diode (LED) array in Panel F3. After selecting the desired channels, solenoid valves were activated by pressing 'Aspiration On/OFF' and 'Aspiration Set Coils' sequentially. To deactivate the selected channels, the user can press again ‘Aspiration On/OFF’ and ‘Aspiration Set Coils’ sequentially.